2007 IEEE International Conference on
Robotics and Automation
Roma, Italy, 10-14 April 2007

Design and Evaluation of a Linear Haptic Device

L. Barbé, B. Bayle, J. Gangloff, M. de Mathelin
LSIIT, UMR ULP-CNRS 7005
Pole API, Bd. S. Brant, 67412 Illkirch, France
(barbe,bayle,jacques,demath)@eavr.u-strasbg.fr

O. Piccin
LGeCo, INSA-Strasbourg
67084 Strasbourg, France
Olivier.Piccin@insa-strasbourg.fr

***Abstract*—The commercial development of haptic devices is very promising. Existing systems are often 6-degree-of-freedom mechanisms equipped with a stylus that acts as a tool. They exhibit force feedback for 3 or 6 degrees of freedom of their end-effector, depending on whether only forces or both forces and torques are rendered. Some planar devices are also used but oddly, one-degree-of-freedom linear haptic devices are quite rare. This lack can probably be explained by the necessary mechanical transformations that are required to achieve linear motions with rotary motors. In this paper, we review several possible structures and present the design of a new one-degree-of-freedom linear haptic device with a limited number of joints and a compact design, compatible with rotary actuation. We evaluate this device in the telemanipulation context.**

I. Introduction

In recent years, robotic telemanipulation and haptics have become very active fields of interest for research, notably in medical applications. In surgery, the first commercial telemanipulators have been dedicated to laparoscopic interventions. However, the pioneer Zeus and da Vinci systems [1] have been equipped with a visual endoscopic feedback, but not with force feedback. Nevertheless, as it allows to feel the interaction forces with the organs, appropriate force feedback would necessarily augment the patient's safety during a teleoperated surgical act. In interventional radiology, another potential application for medical robotics [2], translational force feedback systems would allow to protect the physician from CT-scan radiations while providing him with the perception of the needle penetration through the successive tissues. However, again, no such force feedback systems are available.

To achieve effective medical force feedback telemanipulation in these different domains, the design of specialized systems is commonly preferred to the use of generic robots or devices. Concerning haptic interfaces, which are the purpose of this paper, existing systems are generally 6-degree-of-freedom (DOF) devices equipped with a stylus that stands for the remote or the virtual manipulated tool. Most commercial products generally exhibit force feedback for 3 or 6 DOF of their end-effector, depending on whether only forces or both forces and torques are rendered [3], [4], [5]. Some planar devices, typically pantographs, are also used, principally for research purposes [6], [5] or with special applications. Nevertheless, simple 1-DOF linear haptic devices are quite rare. Yet, such a device would necessarily fulfill the requirements of numerous applications. Among the medical fields already evoked, force feedback needle teleoperated insertions would naturally require such a system. In its absence, the only solution is to use general purpose devices with more DOF and to impose force feedback guidance along a particular direction, what is generally termed as the virtual fixtures approach [7]. Though these techniques already demonstrated interesting results in medical applications [8] , it is natural to believe that, however, they are less effective than the use of a dedicated system. In particular, the ergonomics of a general purpose haptic device is clearly questionable for very fine manipulations.

The lack of large stroke 1-DOF linear devices could be explained by their paradoxical mechanical complexity. Indeed, two solutions are possible to build a linear displacement device. The first one is to use a linear electric actuator [9], but this technology has some disadvantages: linear actuators have generally a bad volume/motion range ratio. Moreover, they are composed of a long magnetic stator track (primary), that is necessarily as long as the necessary rotor (secondary) movement (for up-to-date technological examples, see [10]). Of course, the second and by far the most usual choice is to use rotary motors. However, actuating a translating system with one or several rotary motors requires the design of a mechanism to achieve the motion transformation. This is a quite common problem in mechanical design and many solutions already exists. Generally, it involves either an important number of joints or systems with gears. For this reason, in the case of haptic devices, the mechanical designer necessarily has to answer whether it is compatible with the required performances: limited friction, low inertia, compactness of the mechanism and of the power supply and, if possible, small price.

In this paper we present a novel 1-DOF linear haptic device, initially developed for the teleoperation of needle insertions, and its evaluation in this context. Though the specifications of the system are given for this particular application, we believe that its mechanical principles are original and reproducible. So, the proposed solution can clearly be reused in the design of linear haptic feedback interfaces that require a high force/volume ratio.

II. Existing systems and preliminary solution

A. Specifications

The main function of a haptic device is to provide an adequate interface to give an optimal immersion of the

operator in the remote or the virtual scene. The definition of the specifications of such a system may correspond to a special task, as it is done in the next paragraph. If the considered device is a generic one, the system will have some specificities that determine its possible applications. Typically, the exertable forces and the device workspace are the most determining technical specifications. Then, its resolution in terms of minimum measurable linear and angular motions are generally given. Less often, perceptible force resolution can be estimated, together with the perceived inertia. The friction is generally evaluated by the user when using the device. However, these two last specificities can also be highlighted by an adequate experiment.

To precise the specifications used in the design of the presented prototype, we give the required key features for an haptic device dedicated to needle insertion teleoperation. During manual interventional radiology procedures, the radiologist can exert axial forces up to 20 N [11]. This maximum effort occurs in specific procedures like vertebroplasties when the needle is in contact with bones. However, for most other medical procedures, which correspond to soft tissues interactions, the force range is approximatively bounded to 10 N. The maximization of the stroke is also a major factor to improve realism. Medical practitioners consider that a value of at least 100 mm is required to mimic the needle insertion gesture. Finally, even if the translational motion along the needle axis is the main mobility requirement for percutaneous procedures, the possibility to rotate properly the bevel of the needle is sometime useful to slip over anatomic obstacles during insertion. As a result, the haptic interface necessarily features one translational DOF with force feedback plus an additional passive rotary motion about the previous axis for bevel orientation. This self rotation is not a basic requirement of the system design but it can be achieved easily at the end-effector level. Concerning the ergonomics, due to the variety of possible hand positions and needle incidences that must be accommodated, the device has to be easily re-oriented. Also, it has to be compact to achieve a minimal intrusion in the operator's workspace. The main functional requirements for the haptic device are summarized on the FAST diagram in Fig. 1.

If we consider the previous paragraph, we can estimate that the required specifications correspond to a device for which the exertable force and the ratio workspace/volume are both relatively high. This latter point is often obtained with haptic devices such as those of the PHANTOM family, whose extent is very good thanks to their anthropomorphic structure. However, compactness and force requirements are generally contradictory. In a sense, this compromise is the key specification of the proposed design. It could of course be claimed in a large number of applications.

B. Existing standard solutions and preliminary design

In this paper, we set out to design a mechanical architecture providing the required motion and force transmission. It is a standard approach in mechanism design to think in terms

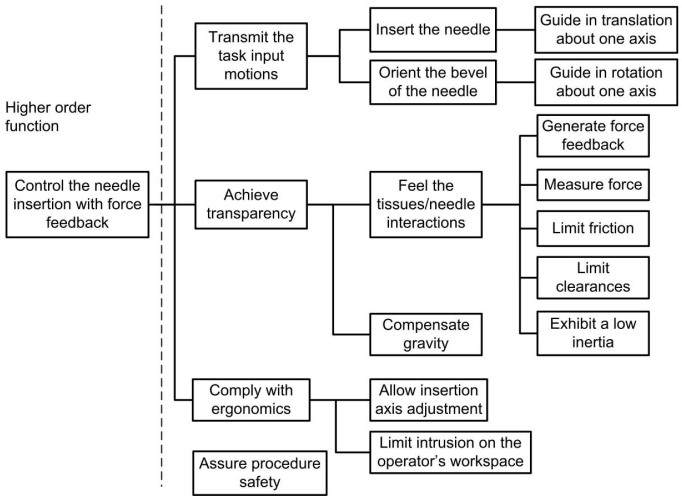

Fig. 1. FAST diagram of a haptic interface dedicated to teleoperated needle insertions.

of elementary building blocks to produce a particular motion function [12]. Basically, the mechanism design problem can be stated as converting a rotary input motion into generating a straight line path. Screw mechanism, rack-and-pinion, cam follower, cable-pulley and slider-crank are the main elementary building blocks available for this task. To cope with the force capability demanded at the device output, such basic mechanisms are generally associated to a transmission. Classical transmissions for haptic interface include mainly gear train cable-pulley with capstan.

In the preliminary design stages, we first selected four possible architectures based on a rack-and-pinion system, a pantograph linkage, a cable and pulleys mechanism and a slider-crank. When comparing the relative merits of these transmission techniques it was found that the rack-and-pinion system and the pantograph linkage were not appropriate mechanisms mainly for reasons of bulk (and complexity for the pantograph linkage).

Additional investigation was carried out on a cable and pulleys mechanism driven via a capstan. A preliminary design of this transmission was studied. Its CAD model is presented in Fig. 2. The motor shaft 5 is connected to the pulley 4 with a capstan. The driven pulley motion is transmitted to the fixed idler 3 via an open-ended cable. A carriage 2, holding the end-effector rod 1 and guided on a slider, is attached to the cable to allow the output translational motion. This embodiment achieves an operating stroke of 120 mm which is satisfactory for the application requirements. However, the resulting bulk of the interface could not be less than 300 mm in height.

To solve this problem, a system based on a slider-crank mechanism could be a promising design solution to improve the compactness of the device. The resulting system is a backdrivable mechanism operated by the human operator in which a rotary motor provides the force feedback to simulate

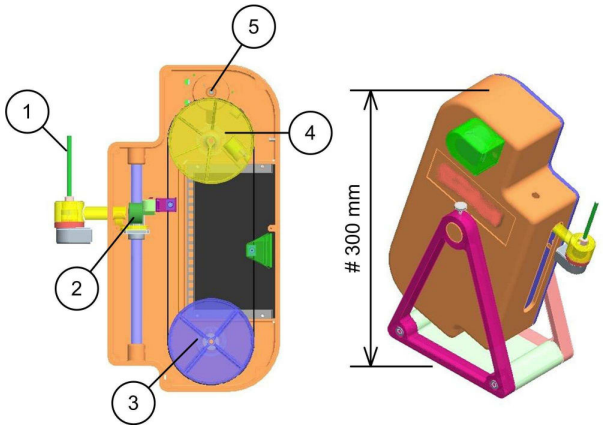

Fig. 2. Preliminary design of the interface.

the interaction of the needle with a tissue.

III. Mechanical Structure and Modeling

A. Structure description

A schematic representation of the mechanism is presented in Fig. 3. The crank S_1 is actuated via a capstan by a rotary motor. The slider S_3 to which the handle is rigidly connected can be moved by the operator and presents a needle-like interface to the human hand. Point P denotes the handle tip.

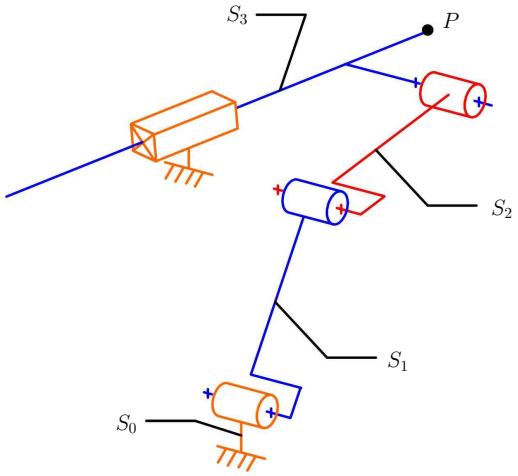

Fig. 3. Kinematical structure of the device.

B. Modeling

1) Notations and parameterization: Vectors are typed in bold face. A vector defined from point A_1 to point A_2 is denoted by $\mathbf{A_1A_2}$. For any $i, j = 1,\ 2,\ 3$, s_i and c_i denote the sine and cosine of q_i. Likewise s_{i-j} and c_{i-j} denote the sine and cosine of $q_i - q_j$.

The slider-crank mechanism is composed of four links S_i namely the ground S_0, the crank S_1, the connecting rod S_2 and the slider S_3. Link lengths are noted l_i. A reference frame $\mathcal{F}_i = \{A_i; \mathbf{x}_i, \mathbf{y}_i, \mathbf{z}_0\}$ is attached to the link S_i with its origin located as indicated in Fig. 4. Vector $\mathbf{x}_i$ is directed from the proximal to the distal end of link i. The mechanism is parameterized by q_1, q_2, q_3 and r as follows:

- Link angular positions are measured with respect to $\mathbf{x}_0$ with parameters $q_i = (\mathbf{x}_0, \mathbf{x}_i)$. Note that q_3 is a known constant parameter that can be adjusted when orienting the interface before startup.
- Point A_{ref} denotes the position of the point A_2 when the mechanism is in its initial configuration. This point A_{ref} will serve as a reference to locate the position of the distal point P. The tool tip position P is measured with respect to A_{ref} such that $\mathbf{A_{ref}P} = r_p\mathbf{x}_3$. Point A_{ref} (and subsequently, variable r_p) is convenient to specify the tool tip displacement but is not coincident with the point A_2 of the slider. Equations derivation is easier when considering A_2.
- The variable $r = \mathbf{A_0A_2} \cdot \mathbf{x}_3$ is introduced to derive the geometric model. It is related to r_p by the relation $r_p = r - r_{A_{\text{ref}}} + l_3$.

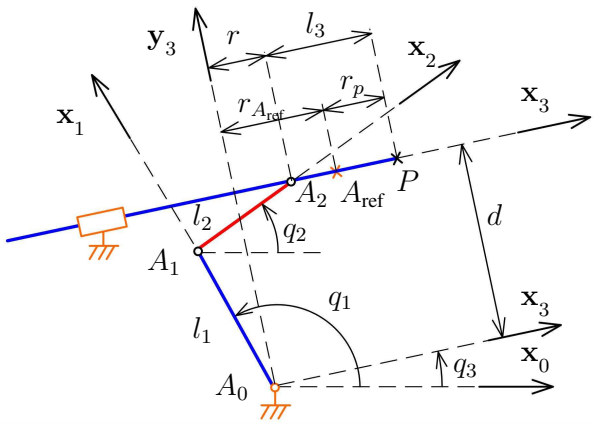

Fig. 4. System frames and parameterization.

q_1 and r are the input/output variables for this 1-DOF mechanism.

2) Position analysis: The loop closure equation projected on $\mathcal{F}_0$ writes

$$l_1c_1 + l_2c_2 = rc_3 - d\,s_3 \quad (1)$$
$$l_1s_1 + l_2s_2 = rs_3 + d\,c_3 \quad (2)$$

r is supposed to be the input variable so that q_1 is the unknown. The elimination of the intermediate variable q_2 can be performed using the previous equations and leads to an equation of the form

$$Ac_1 + Bs_1 = D \quad (3)$$

where $A = 2l_1(d\,s_3 - rc_3)$, $B = -2l_1(d\,c_3 + rs_3)$ and $D = l_2^2 - d^2 - l_1^2 - r^2$ can be calculated.

To solve equation (3), the trigonometric half-angle identities for sine and cosine can be used. With $t = \tan\frac{q_1}{2}$, equation (3) is transformed into the the following quadratic expression in t:

$$(A+D)t^2 - 2Bt - (A-D) = 0 \tag{4}$$

Solving for t and q_1 gives

$$q_1 = 2\arctan\frac{B + \sigma\sqrt{B^2 - D^2 + A^2}}{A+D} \tag{5}$$

where the sign variable $\sigma = \pm 1$ identifies the assembly mode of the mechanism. In practice, the solutions of equation (4) are real otherwise the mechanism is in a configuration (set by the value of r) that can not be assembled. There are two solutions for q_1 corresponding to the two values of σ. Here, the valid assembly mode is obtained for a value of q_1 in the range $[0;\pi]$.

Now, q_2 can be calculated from equations (1) and (2) as follows:

$$q_2 = \arctan\frac{rs_3 + d\,c_3 - l_1 s_1}{rc_3 - d\,s_3 - l_1 c_1} \tag{6}$$

3) Velocity analysis: The differentiation of equations (1) and (2) leads to the value of $\dot{r}$, that can be calculated when not in singular configuration (links 2 and 3 orthogonal):

$$\dot{r} = l_1\frac{s_{2-1}}{c_{2-3}}\dot{q}_1 \tag{7}$$

The value of $\dot{q}_1$ is obtained by the inversion of the previous equation.

The quasi-static evolution of the actuation torque acting on the crank is given in Fig. 5 for several values of the force F_h applied to the end-effector along $\mathbf{x}_3$. The obtained torque has a quasi-linear limited variation in the operation range of parameter r.

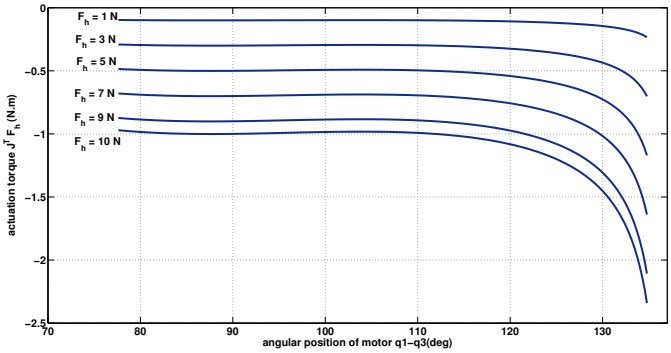

Fig. 5. Actuation torque during tip displacement.

4) Dynamic model: In this section, we derive the dynamic equations of the device. We choose to write the Lagrange equations with multiplier using the parameters q_1 and q_2. As the system has 1-DOF with two parameters $\mathbf{q}$, the equations can be written using one multiplier λ:

$$\frac{d}{dt}\frac{\partial T}{\partial \dot{\mathbf{q}}} - \frac{\partial T}{\partial \mathbf{q}} = \mathbf{Q} - \frac{\partial V}{\partial \mathbf{q}} + \phi^T\lambda \tag{8}$$

where T and V denote the kinetic and potential energy. The vector $\mathbf{Q} = \begin{pmatrix}\tau_m & 0\end{pmatrix}^T$ includes the external actions applied to the system, namely the actuator torque τ_m.

The kinematic constraint equation between the variables q_1 and q_2 can be derived from (1) and (2) and written:

$$\phi^T\dot{\mathbf{q}} = 0 \tag{9}$$

with $\phi = \begin{pmatrix}l_1 c_{1-3} & l_2 c_{2-3}\end{pmatrix}^T$.

Upon calculation, equation (8) is written:

$$M(\mathbf{q})\ddot{\mathbf{q}} + C(\mathbf{q})\dot{\mathbf{q}}^2 = \mathbf{Q} + \mathbf{G}(\mathbf{q}) + \phi^T\lambda \tag{10}$$

where A, B and G represent the matrices of inertial, centrifugal and gravity effects. The following expressions are obtained:

$$M(\mathbf{q}) = \begin{pmatrix} XX & XYc_{1-2} \\ XYc_{1-2} & YY\end{pmatrix}$$

$$C(\mathbf{q}) = XYs_{1-2}\begin{pmatrix}0 & 1\\ -1 & 0\end{pmatrix}$$

$$\mathbf{G}(\mathbf{q}) = \begin{pmatrix}h_1 c_1 \\ h_2 c_2\end{pmatrix}$$

where

$$XX = m_1 l_{G_1}^2 + (m_2+m_3)l_1^2 + J_1^{zz} \tag{11}$$
$$XY = l_1(m_2 l_{G_2} + m_3 l_2) \tag{12}$$
$$YY = m_2 l_{G_2}^2 + m_3 l_2^2 + J_2^{zz} \tag{13}$$
$$h_1 = (m_1 l_{G_1} + (m_2+m_3)l_1)g \tag{14}$$
$$h_2 = (m_2 l_{G_2} + m_3 l_2)g \tag{15}$$

The dynamic model (10) can then be written:

$$\Theta^T W(\mathbf{q},\dot{\mathbf{q}},\ddot{\mathbf{q}}) = \tau_m \tag{16}$$

where

$$\Theta = \begin{pmatrix}XX & YY & XY & h_1 & h_2\end{pmatrix}^T$$

$$W = \begin{pmatrix} \ddot{q}_1 \\ -\alpha\ddot{q}_2 \\ c_{1-2}\left(\ddot{q}_2 - \alpha\ddot{q}_1\right) + s_{1-2}\left(\dot{q}_2^2 + \alpha\dot{q}_1^2\right) \\ c_1 \\ -\alpha c_2\end{pmatrix}$$

By differentiating the position equations (1) and (2), the expression of $\ddot{q}_2$ can be derived in function of $\dot{q}_1$:

$$\dot{q}_2 = -\alpha\dot{q}_1$$
$$\ddot{q}_2 = -\alpha\ddot{q}_1 + \beta\dot{q}_1^2$$

where

$$\alpha = \frac{l_1}{l_2}\frac{c_{1-3}}{c_{2-3}} \qquad \beta = \frac{l_1}{l_2}\frac{1}{c_{2-3}}\left(s_{1-3} + \frac{l_1}{l_2}\frac{s_{2-3}}{c_{2-3}}c_{1-3}^2\right)$$

5) Dynamic parameters identification: For the controller implementation, the dynamic parameters were either identified or estimated from CAD Software. The obtained parameters are given in the following table.

	CAD parameters	Estimated parameters
XX $(kg \cdot m^2)$	$14.85 \cdot 10^{-4}$	$15.9 \cdot 10^{-4}$
XY $(kg \cdot m^2)$	$2.62 \cdot 10^{-4}$	$2.1 \cdot 10^{-4}$
YY $(kg \cdot m^2)$	$0.78 \cdot 10^{-4}$	$2.0 \cdot 10^{-4}$
h_1 $(kg \cdot m^2 \cdot s^{-2})$	0.1209	0.1440
h_2 $(kg \cdot m^2 \cdot s^{-2})$	0.0257	0.0119

TABLE I
NUMERICAL VALUES OF DYNAMICS PARAMETERS OF HAPTIC INTERFACE.

C. Prototype

A CAD view of the overall system and the first prototype are given in Fig. 6. This design features a stroke of 115 mm with a motor angular displacement included in 77.6 deg and 136.3 deg in order to avoid singularities. The complete device including servoamplifier and power supply fits in an orientable $195 \times 180 \times 155$ mm box. The volume of the prototype has been clearly reduced compared to our initial design (about -50%). The system is equipped with a force cell that allow any kind of teleoperation structure, and is also usefull for performance evaluation. Force up to 18 N peak values were finally obtained and a continuous force of 7 N can be applied, and the resolution of force measurement is 0.0122 N. Controller software is based on a real-time Linux that allows sampling rates up to 7 kHz.

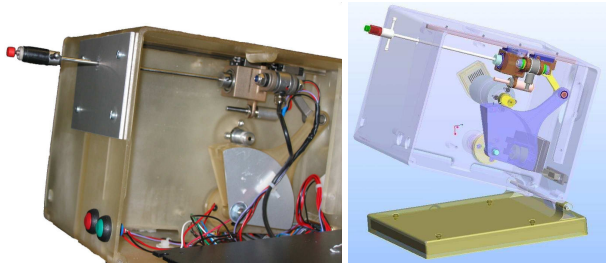

Fig. 6. (a) Prototype and (b) CAD view.

IV. PRELIMINARY EXPERIMENTS

A. Teleoperation structure

The fundamental requirements for telemanipulation systems are stability and transparency [13]. Several techniques allow to evaluate these characteristics for a given bilateral controller in spite of time delays, plant disturbances, measurements noise and modeling uncertainties [14], [15], [16]. In this paper we choose to evaluate the designed haptic device with a force-position scheme [14]. The position of the master manipulator is the reference for the slave manipulator, i.e. $x_s^d = x_m$ and, reciprocally, the force measured when the slave is in contact with the environment is the reference for the master manipulator, i. e. $f_h^d = f_{env}$. If it is required, force and position can be scaled to allow the amplification of motions or forces.

The master controller is a proportional-integral controller with a feedforward term of the desired force, with gravity effects compensation, defined by the following law [17], [18]:

$$u_m = \hat{g}(q_1) + J^T \left(f_h^d + K_f (f_h^d - f_h) + \frac{1}{T_i} \int (f_h^d - f_h) d\tau \right)$$

with $\hat{g}(q_1) = h_1 c_1 - \alpha h_2 c_2$. The slave controller is a proportional controller defined by the following law :

$$u_s = K_p (x_s^d - x_s)$$

The implementation of the force-position scheme is represented in Fig. 7.

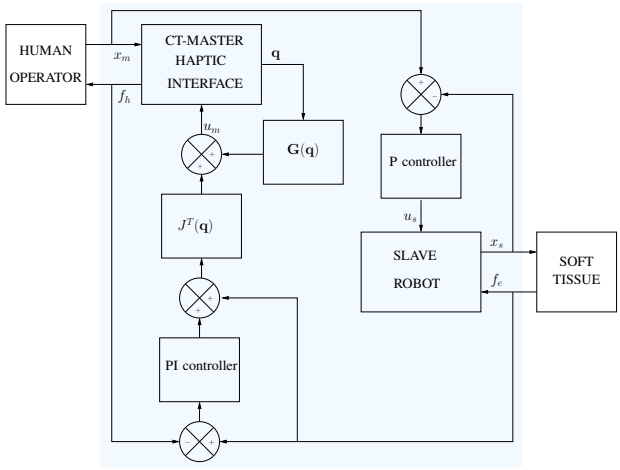

Fig. 7. Force-Position control scheme.

B. Results

In the proposed experiments, the slave manipulator is a Cartesian robot equipped with an ATI force sensor. A surgical needle is attached to its end-effector. We use an abdominal phantom, customized with additional artificial skins in order to amplify rupture effects. The controller gains were tuned and tested in simulation. This tuning was achieved from the dynamic model of the haptic interface for the master controller and with an identified model of the slave robot, for the slave controller. As one can observe in Fig. 8, the forces measured on the haptic device correspond very accurately to the forces measured when the translating needle perforates the different layers of the mannequin. These transitions are characterized by rapid force variations at time $t = 2$ s and $t = 6.5$ s. Then, a relaxation phase and finally the needle extraction are perceived in a very realistic manner. The difference between the forces measured on the master and the slave are characterized by an absolute mean value of 0.147 N, with a standard deviation of 0.137 N. The worst transient error of 1.19 N happens when the needle is extracted, and corresponds to a 2.8 N step. Concerning position tracking, the interaction of the slave with the soft material creates a very limited perturbation. The absolute mean value of the

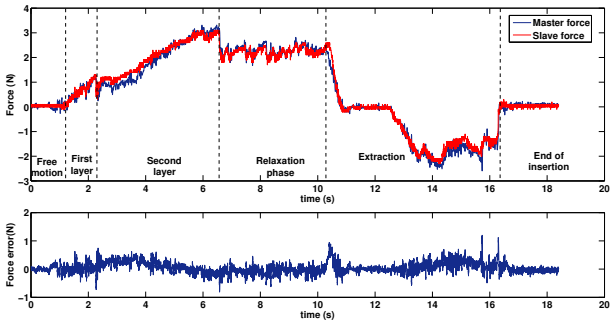

Fig. 8. Master/Slave forces during a needle insertion into a multi-layer soft material. Associated force tracking error.

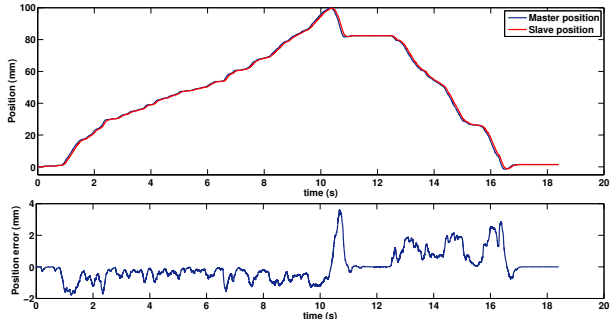

Fig. 9. Master/Slave positions during a needle insertion into a multi-layer soft material. Associated position tracking error.

position tracking error is 0.65 mm. However, some transients during tissue rupture create up to 4 mm errors. So, even if it was not the goal of this paper, it is clear that force feedback teleoperation of needle insertions is also a challenging control problem, that should certainly require a more sophisticated solution.

V. Conclusion

In this paper, we have adapted the slider-crank principle to design a novel 1-DOF haptic device. Though specified for a particular medical application, this system can easily be used for applications that require both high forces and a good ratio workspace/volume. The proposed solution is based on a conventional rotary motors technology and restricts mechanically the motion of the system to a pure translation with limited friction. The building of a the prototype adapted to needle insertion teleoperation specifications was presented. Its use in the context of a teleoperation task allows to obtain a very good force and position behavior, which illustrates the system transparency.

This work open several perspectives, both for improvements and for future designs. The complete identification of the dynamic parameters will be studied in near future, in order to improve the dynamic model, which is used in the system controller. Finally, as a general perspective in haptic devices design, innovative rotary or linear actuation technologies should be considered to obtain real innovations in this domain.

Acknowledgment

This work was supported by the Alsace Regional Council and the CNRS.

References

[1] Intuitive Surgical Inc., "The da vinci surgical system," 2006. http://www.intuitivesurgical.com/products/index.aspx.

[2] D. Stoianovici, L. L. Whitcomb, J. H. Anderson, R. H. Taylor, and L. R. Kavoussi, "A modular surgical robotic system for image guided percutaneous procedures," in *Medical Image Computing and Computer-Assisted Intervention*, (Cambridge, USA), October 1998.

[3] SensAble Technologies, "Phantom devices," 2006. http://www.sensable.com/products/phantom_ghost/phantom.asp.

[4] Force Dimension, "Delta haptic devices," 2006. http://www.forcedimension.com/fd/avs/home/products.

[5] Quanser Inc., "Quanser haptic devices. product information," 2006. http://www.quanser.com/industrial/html/products/fs_products.asp.

[6] C. Ramstein and V. Hayward, "The pantograph: a large workspace haptic device for a multi-modal humancomputer interaction," in *Conference on Human Factors in Computing Systems*, (Boston, USA), April 1994.

[7] L. Rosenberg, "Virtual fixtures: Perceptual tools for telerobotic manipulation," in *IEEE Virtual Reality International Symposium*, pp. 76–82, 1993.

[8] A. Bettini, S. Lang, A. Okamura, and G. Hager, "Vision assisted control for manipulation using virtual fixtures," in *IEEE/RSJ International Conference on Intelligent Robots and Systems*, pp. 1171–1176, 2001.

[9] I. Boldea and S. Nasar, "Linear electric actuators and generators," *IEEE Transactions on Energy Conversion*, vol. 14, pp. 712 – 717, September 1999.

[10] Rockwell Automation, "Anorad – linear motion solutions," 2006. http://www.rockwellautomation.com/anorad.

[11] B. Maurin, L. Barbe, B. Bayle, P. Zanne, J. Gangloff, M. de Mathelin, A. Gangi, and L.Soler, "In vivo study of forces during needle insertions," in *Proceedings of Medical Robotics, Navigation and Visualisatoin Scientifc Workshop*, (Remagen, Germany), March 2004.

[12] A. G. Erdman, G. N. Sandor, and S. Kota, *Mechanism Design - Analysis and Synthesis*. Prentice Hall, 2001.

[13] D. Lawrence, "Stability and transparency in bilateral teleoperation," *IEEE Transaction on Robotics and Automation*, vol. 9, pp. 624–637, October 1993.

[14] B. Hannaford, "Design framework for teleoperators with kinesthetic feedback," *IEEE Transactions on Robotics and Automation*, vol. 5, pp. 426–434, August 1989.

[15] R. Anderson and M. Spong, "Bilateral control of teleoperators with time delay," *IEEE Transactions on Automatic Control*, vol. 34, pp. 494–501, May 1989.

[16] G. Niemeyer and J.-J. Slotine, "Stable adaptive teleoperation," *Journal of oceanic engineering*, vol. 16, pp. 152–162, January 1991.

[17] S. Chiaverini, B. Siciliano, and L. Villani, "A survey of robot interaction control schemes with experimental comparaison," *IEEE/ASME Transaction on Mechatronics*, vol. 4, pp. 273–285, Spetember 1999.

[18] D. Whitney, "Force feedback control of manipulator fine motions," *Transaction ASME Journal of Dynamics Sytem, Measure and Control*, vol. 99, pp. 91–97, 1977.